

Off-resonant defocus-contrast imaging of cold atoms

Lincoln D. Turner, Karl P. Weber, David Paganin,* and Robert E. Scholten

School of Physics, University of Melbourne, Victoria 3010, Australia

Received June 16, 2003

We demonstrate the retrieval of column-density images of cold atoms, using a noninterferometric phase-recovery technique based on a single off-resonant and defocused intensity image. The quantitative column density is retrieved via Fourier inversion and remains robust with respect to detuning and defocus. The technique offers excellent prospects for simple, nondestructive imaging of atoms in magnetic and optical traps and condensates. © 2004 Optical Society of America
OCIS codes: 100.5070, 120.5050, 350.5030.

Optical imaging provides a powerful diagnostic method for a diverse range of experiments involving cold atoms. On-resonant absorption imaging is predominant, despite its limited dynamic range and recoil heating. Off-resonant phase-imaging techniques have allowed nondestructive and quantitative imaging of Bose–Einstein condensates^{1,2} (BECs), but conventional approaches require precisely aligned phase plates or interferometers. We describe how one may exploit Fresnel diffraction of an off-resonant probe beam to observe weakly absorbing cold atoms in phase contrast, using a standard absorption imaging configuration modified only by a small defocus of the imaging lens.

Off-resonant imaging relies on rendering phase shifts into intensity variations measurable with a CCD detector. Interferometry is the classic approach, for example, in the recent implementation of off-axis digital holography,³ but it is awkward to construct and align an interferometer around a cold atom sample. The Zernike phase-contrast technique⁴ forms a common-path interferometer in which the background unscattered wave serves as the interferometric reference. A $\pi/2$ phase plate inserted in the Fourier plane of an image relay system shifts the phase of the unscattered probe wave so that it interferes with the field retarded by the atoms to produce a phase-contrast image. Difficulties associated with precise fabrication of the phase plate and exacting alignment requirements have impeded the application of the Zernike method to atom imaging.¹

The Zernike phase plate produces an intensity signal that is approximately linear in the phase shift for small phase shifts. A phase-contrast signal is also produced through Fresnel diffraction. The effect is familiar in optical microscopy, where dark and bright contours appear at the edges of a transparent object (e.g., a cell, an optical fiber) at the slightest defocus. The diffracted intensity image can be compared to a calculated diffraction pattern and hence used to fit the atom column density.⁵ Absorption and phase-shift information can also be retrieved directly from the Fresnel diffraction pattern by inverse methods. In particular, a solution was recently derived for the special case of x-ray imaging of homogeneous samples, where absorption and phase retardation are both functions only of the object thickness.⁶ Here we outline this result as applied to the retrieval of a

column-density image of cold atomic gas from a single defocus-contrast image.

A probe beam propagates through the atom cloud and diffracts in the free space beyond (Fig. 1). The probe beam is described as a scalar plane wave of complex amplitude U_{in} propagating along the z axis, incident on an object with a spatial distribution of complex refractive index $n(\mathbf{r}, z)$. For an optically thin object, the amplitude over the exit plane is

$$U(\mathbf{r}, z = 0) = U_{\text{in}} \exp\left\{ik_0 \int [n(\mathbf{r}, z) - 1] dz\right\}, \quad (1)$$

where $k_0 = 2\pi/\lambda_0$ is the wave number for vacuum probe wavelength λ_0 and $\mathbf{r} \equiv (x, y)$ are the transverse coordinates.

The complex refractive index for a sample of two-level atoms with number density $\rho(\mathbf{r}, z)$ can be written as⁷

$$n(\mathbf{r}, z) = 1 + \frac{3\lambda_0\rho(\mathbf{r}, z)}{2k_0^2} \left(\frac{i - 2\delta}{1 + 4\delta^2} \right), \quad (2)$$

$$\equiv 1 + \rho(\mathbf{r}, z) (n_r + in_i). \quad (3)$$

n_r and n_i are the real and the imaginary refractive-index components normalized to the atomic density and relative to vacuum, and δ is the detuning in full linewidths; it follows that $n_r/n_i = -2\delta$. We wish to measure the integrated column density of the sample, $\rho(\mathbf{r}) = \int \rho(\mathbf{r}, z) dz$. The intensity I and phase ϕ of the field at the exit plane are

$$I(\mathbf{r}, z = 0) = |U(\mathbf{r}, z = 0)|^2 = I_{\text{in}} \exp[-2k_0n_i\rho(\mathbf{r})], \quad (4)$$

$$\phi(\mathbf{r}, z = 0) = k_0n_r\rho(\mathbf{r}), \quad (5)$$

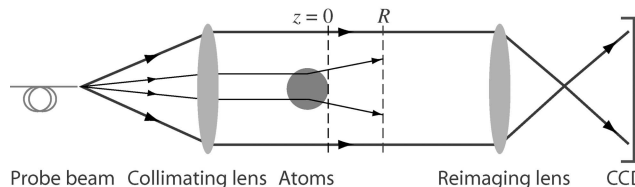


Fig. 1. Schematic of the imaging configuration. A cloud of ⁸⁵Rb atoms was illuminated with a fiber-coupled and collimated laser beam detuned from resonance. A lens reimaged the light from a plane at defocus distance R onto a CCD. Rays illustrate the antilensing for above-resonance illumination.

where $I_{\text{in}} = |U_{\text{in}}|^2$. Equation (4) is the familiar Beer-Lambert law, the basis of absorption imaging.

The paraxial wave equation implies a continuity equation, known as the transport-of-intensity equation⁸

$$\nabla_{\perp} \cdot [I(\mathbf{r}, z) \nabla_{\perp} \phi(\mathbf{r}, z)] = -k_0 \frac{\partial}{\partial z} I(\mathbf{r}, z), \quad (6)$$

where ∇_{\perp} is the gradient operator in the transverse plane. Substituting from Eqs. (4) and (5) and evaluating at the plane $z = 0$, this may be written in terms of $\rho(\mathbf{r})$ as

$$\frac{n_r}{2k_0 n_i} I_{\text{in}} \nabla_{\perp}^2 \exp[-2k_0 n_i \rho(\mathbf{r})] = \frac{\partial}{\partial z} I(\mathbf{r}, z = 0). \quad (7)$$

We approximate the intensity derivative $\partial I(\mathbf{r}, z = 0)/\partial z$ as the finite difference $[I(\mathbf{r}, z = R) - I(\mathbf{r}, z = 0)]/R$, where $I(\mathbf{r}, z = 0)$ is given by Eq. (4), so

$$\left(1 - \frac{R\delta}{k_0} \nabla_{\perp}^2\right) \exp[-2k_0 n_i \rho(\mathbf{r})] = \frac{I(\mathbf{r}, z = R)}{I_{\text{in}}}. \quad (8)$$

Equation (8) may be inverted in Fourier space, such that the Laplacian ∇_{\perp}^2 becomes a multiplication by $-|\mathbf{k}|^2$, where $\mathbf{k} = (k_x, k_y)$ is the spatial frequency vector in the transverse plane. The column density is then recovered by deconvolution:

$$\exp[-2k_0 n_i \rho(\mathbf{r})] = \mathcal{F}^{-1} \left\{ \frac{\mathcal{F}\{I(\mathbf{r}, z = R)/I_{\text{in}}\}}{1 + \frac{R\delta}{k_0} |\mathbf{k}|^2} \right\}. \quad (9)$$

That is, to find the column density, the defocused image is Fourier transformed, the Fourier coefficients are reweighted, and the inverse Fourier transform is taken. The result is a synthetic in-focus absorption image, which is then converted to a column density $\rho(\mathbf{r})$ by taking the logarithm; setting $R = 0$ recovers the Beer-Lambert case. Provided that the product $R\delta$ is positive, the denominator is greater than unity and the deconvolution is a well-posed inverse problem.

Figure 1 depicts our apparatus. A sample of cold atoms was generated by a conventional magneto-optical trap⁹ (MOT) with a getter source. The trap accumulated 6×10^5 ^{85}Rb atoms in a nearly Gaussian cloud of FWHM $230 \pm 9 \mu\text{m}$ at a peak density of $3.9 \pm 0.4 \times 10^{16} \text{ m}^{-3}$. An imaging laser of 0.5-MHz linewidth was detuned between ± 5 linewidths Γ from the ^{85}Rb $5S_{1/2}(F = 3) \rightarrow 5P_{3/2}(F = 4)$ resonance. The cw probe beam was fiber coupled, linearly polarized, and collimated before passing through the MOT with irradiance of $10 \mu\text{W cm}^{-2}$. The diffracted beam was attenuated by neutral-density filters to reduce the fluorescence contribution and imaged with a 35-mm camera lens (200 mm Micro-Nikkor) onto a CCD (Roper VersArray 1300F, $20\text{-}\mu\text{m}$ square pixels) with a magnification of 1.8. A standard absorption imaging configuration has been altered only by allowing the lens and CCD assembly to translate an adjustable distance R along a rail so that an image of the diffraction pattern at distance R beyond the object was produced on the detector.

We emphasize that the lens serves only to reimage and magnify the intensity pattern from one focal plane

to the other. Identical images could have been acquired without imaging optics, had it been possible to place the bare CCD detector at defocus distance R from the MOT (inside the vacuum chamber in our setup).

We acquired four images at each detuning and defocus: I_{abs} with the MOT and probe beam on, I_{fluoro} with the MOT on and probe off, I_{bright} with the MOT off and probe on, and I_{dark} with both off. The normalized absorption ratio image,

$$\frac{I(\mathbf{r}, z = R)}{I_{\text{in}}} = \frac{I_{\text{abs}} - I_{\text{fluoro}}}{I_{\text{bright}} - I_{\text{dark}}}, \quad (10)$$

includes a correction for fluorescence that would not be required if imaging a nondissipative object such as a BEC. The fluorescence blurred rapidly with defocus and added only a low-level featureless background to the defocused images.

Figure 2 shows a typical defocused image, normalized as above, taken at a detuning $\delta = +3\Gamma$ and a defocus $R = 30 \text{ mm}$. Blue detuning yields a refractive index with the real component less than unity, and so the probe beam is antiparaxial, darkening the center and forming a bright ring around the edges. Red detuned ($\delta < 0$) images yield a more familiar focusing effect, brightening the middle of the image. However, this is where residual absorption is strongest and the effects tend to cancel, causing a loss of contrast related to the singularity in Eq. (9) for negative $R\delta$. If the residual object absorption is significant and red detuning is desired, the lens should be defocused by $-R$, i.e., toward the atom cloud, to ensure positive $R\delta$. The line profile in Fig. 2 shows the extent of the defocus contrast enhancement, comparing focused and defocused images taken at the same detuning. The in-focus absorption contrast of 6% increased to 30% when the image was defocused by 30 mm.

We processed the in-focus image $I(\mathbf{r}, z = 0)/I_{\text{in}}$ (not shown) following Eq. (4) and the normalized defocus image of Fig. 2, $I(\mathbf{r}, z = R)/I_{\text{in}}$, following Eq. (9). Using fast Fourier transforms, we obtained full retrieval of a 512×512 pixel image in less than 1 s on a 1-GHz Pentium processor.

Figure 3 shows the column-density image retrieved from the defocused image and a central line profile compared with the same line retrieved from the in-focus image. The improvement in the signal-to-noise ratio (SNR) is not unexpected given the higher contrast shown by Fig. 2. Users of laser imaging

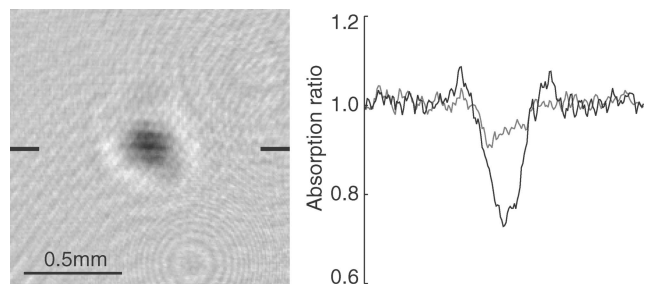


Fig. 2. Defocused image for detuning $\delta = +3\Gamma$ and defocus $R = 30 \text{ mm}$. Line profiles (three-pixel rows averaged) are shown for the defocus image and (gray curve) for a conventional in-focus absorption image at the same detuning.

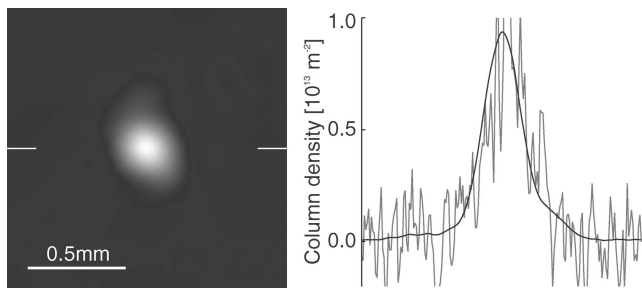


Fig. 3. Column-density gray-scale image retrieved from the defocus image of Fig. 2. Line profiles (single pixel row) are shown for the column density derived from our method compared with that retrieved from conventional in-focus absorption imaging at the same detuning (gray curve).

systems will have noted the remarkable ease with which vacuum windows and lenses align themselves as unwanted interferometers. The resulting spurious fringes are typically at a higher spatial frequency than the majority of structure in the object. The retrieval is biased against high spatial frequencies, rolling off as $|\mathbf{k}|^{-2}$ for large $|\mathbf{k}|$. We found that this inherent denoising successfully suppressed the effects of unintended interference in our imaging system.

We obtained column densities from contrast images at detunings from 0 to $+5\Gamma$ and defocusing ranging from 10 to 40 mm. We also took an in-focus image at each detuning and retrieved the column density with the standard absorption imaging method. As the density of our MOT was relatively low, absorption at $+5\Gamma$ was only 2%, yielding a unity SNR for standard absorption imaging at this extreme detuning. Column densities retrieved from absorption and defocus-contrast images showed good agreement, with the central column density being $9.4 \pm 0.7 \times 10^{12} \text{ m}^{-2}$. Absorption imaging is very sensitive to small errors in focus. As little as 0.5-mm defocus of our imaging system caused a 20% error in the column density retrieved with standard in-focus absorption imaging, whereas the same error in $R = 20$ mm caused negligible error in our defocus-contrast image. Consequently, the peak column densities measured by absorption imaging show greater scatter than the defocus-contrast measurements, which exhibit only small shot-to-shot variation consistent with MOT fluctuations detectable from fluorescence images.

The optimal defocus distance depends on the size and structure of the object being imaged. At zero defocus, there is only residual absorption contrast. The contrast increases linearly with defocus until the finite-difference approximation of the intensity derivative used to obtain Eq. (8) no longer holds. This transition from single fringe contrast to holographic contrast nominally occurs at defocus $R_{\text{max}} = 2\pi^2/\lambda|\mathbf{k}|^2$. Therefore, at any defocus distance R there is an object structure scale $\sqrt{\pi 2\lambda R}$ that is optimally diffracted.¹⁰ Much smaller structures in the object will be in holographic contrast and will be

suppressed by the filter, while much larger structures will show only absorption contrast with little additional defocus contrast.

Of previously reported methods for off-resonant imaging, the Zernike phase-contrast technique is most similar to our defocus-contrast approach. Both our method and the Zernike method are bright-field techniques and so have a SNR superior to those of dark-field methods in the presence of technical noise. Residual absorption by the atom cloud introduces inaccuracies in the Zernike contrast but increases the signal for defocus contrast. The Zernike method has enabled many sequential nondestructive images of a BEC to be taken.¹ Our technique yields lower contrast for all but the optimal spatial frequency component of an image. Equivalently, our technique is somewhat more destructive for the same SNR. Nevertheless, we expect that several sequential nondestructive images of a BEC could be obtained with our method, using only conventional absorption imaging optics.

Our results demonstrate a quantitative off-resonant imaging technique based on defocus contrast. The method uses a standard absorption imaging apparatus but retrieves quantitative column-density images calibrated by knowing defocus distance R and probe detuning δ . We expect that the great simplicity of the technique will lead to the wider use of nonresonant imaging in cold atom research.

This work was supported by the Commonwealth Department of Education, Science and Training Innovation Access Programme and by Australian Research Council grant DP0208799. R. E. Scholten's e-mail address is r.scholten@physics.unimelb.edu.au.

*Present address, School of Physics and Materials Engineering, Monash University, Victoria 3800, Australia.

References

1. M. R. Andrews, M.-O. Mewes, N. J. van Druten, D. S. Durfee, D. M. Kurn, and W. Ketterle, *Science* **273**, 84 (1996).
2. M. R. Andrews, D. M. Kurn, H.-J. Miesner, D. S. Durfee, C. G. Townsend, S. Inouye, and W. Ketterle, *Phys. Rev. Lett.* **79**, 553 (1997).
3. S. Kadlecik, J. Sebby, R. Newell, and T. G. Walker, *Opt. Lett.* **26**, 137 (2000).
4. F. Zernike, *Physica* **9**, 686 (1942).
5. F. Strauch, V. Gomer, H. Schadwinkel, B. Ueberholz, D. Haubrich, and D. Meschede, *Opt. Commun.* **145**, 57 (1998).
6. D. Paganin, S. C. Mayo, T. E. Gureyev, P. R. Miller, and S. W. Wilkins, *J. Microsc. (Oxford)* **206**, 33 (2002).
7. W. Demtröder, *Laser Spectroscopy*, 2nd ed. (Springer-Verlag, Berlin, 1981).
8. M. R. Teague, *J. Opt. Soc. Am.* **73**, 1434 (1983).
9. E. L. Raab, M. Prentiss, A. Cable, S. Chu, and D. E. Pritchard, *Phys. Rev. Lett.* **59**, 2631 (1987).
10. A. Pogany, D. Gao, and S. W. Wilkins, *Rev. Sci. Instrum.* **68**, 2774 (1997).